Multi-scale thermal homeostasis: Plants achieve temperature control through hierarchical regulation

Yuqiang Jiang

yqjiang@genetics.ac.cn

Laboratory of Integrative Physiology, Institute of Genetics and Developmental Biology, Chinese Academy of Sciences

xia chen

Laboratory of Integrative Physiology, Institute of Genetics and Developmental Biology, Chinese Academy of Sciences

Chao Li

Laboratory of Integrative Physiology, Institute of Genetics and Developmental Biology, Chinese Academy of Sciences

Rongcheng Han

Laboratory of Integrative Physiology, Institute of Genetics and Developmental Biology, Chinese Academy of Sciences

Fan Chen

Institute of Genetics and Developmental Biology https://orcid.org/0000-0003-4482-3116

Lu Huang

Laboratory of Integrative Physiology, Institute of Genetics and Developmental Biology, Chinese Academy of Sciences

Dianying Zhao

Laboratory of Integrative Physiology, Institute of Genetics and Developmental Biology, Chinese Academy of Sciences

Yuxiao Wu

South China Normal University

Feihong Yan

Laboratory of Integrative Physiology, Institute of Genetics and Developmental Biology, Chinese Academy of Sciences

Yaqiang Qin

Laboratory of Integrative Physiology, Institute of Genetics and Developmental Biology, Chinese Academy of Sciences

Hao Shi

Laboratory of Integrative Physiology, Institute of Genetics and Developmental Biology, Chinese Academy of Sciences

Yu Wang
Laboratory of Integrative Physiology, Institute of Genetics and Developmental Biology, Chinese Academy of Sciences

---

Article

Keywords:

Posted Date: May 12th, 2026

DOI: https://doi.org/10.21203/rs.3.rs-9602775/v1

Additional Declarations: There is **NO** Competing Interest.

Multi-scale thermal homeostasis: Plants achieve temperature control through hierarchical regulation

Xia Chen[1,2,#], Chao Li[1,2,#], Lu Huang[1,2], Dianying Zhao[1,2], Yuxiao Wu[1,3], Feihong Yan[1,2], Yaqiang Qin[1,2], Hao Shi[1], Yu Wang[1,2], Rongcheng Han[1,2,*], Fan Chen[4], Yuqiang Jiang[1,2,*]

[1] Laboratory of Integrative Physiology, Institute of Genetics and Developmental Biology, Chinese Academy of Sciences, Beijing 100101, China.

[2] University of Chinese Academy of Sciences, Beijing 100049, China.

[3] South China Normal University, Guangzhou 510630, China.

[4]Yazhouwan National Laboratory, Sanya, Hainan 572704, China.

[#] These authors have same contributions to this work.

*Corresponding authors: hanrch@genetics.ac.cn (Rongcheng Han); yqjiang@genetics.ac.cn (Yuqiang Jiang).

Temperature fundamentally impacts plants growth and physiology. However, the mechanisms by which plants sense and response to environmental changes remain unclear due to the lack of effective methods for measuring internal plant temperatures. Here, by combining lab-made nanothermometric probes with time-gated imaging technique, we accurately detected the change in internal plant temperature in response to environmental temperature variations. We discovered a multilevel temperature regulation mechanism during the process by which plants establish thermal homeostasis. In *Nicotiana benthamiana* leaves, when environment temperature changes from approximately 24°C to 45°C, the maximum of internal plant temperature change is only approximately 10°C near cell wall, and less than 7°C in cytoplasm, while remaining nearly constant in chloroplasts ($\Delta T_{chl} \approx 1$°C). Similar compartment-specific thermal regulation was observed in *Arabidopsis thaliana* and tomato, indicating that hierarchical regulation represents a conserved strategy for maintaining internal temperature stability in plants. Together, these findings provide direct evidence for multiscale thermal homeostasis in plants and establish a framework for understanding how cellular and subcellular organization contributes to temperature regulation.

Main

As sessile organisms, plants are generally exposed to fluctuating environmental conditions, among which temperature stress is particularly prominent[1]. Under severe conditions, it may even lead to plant mortality[2,3]. Historically, plants were deemed poikilothermic, incapable of regulating their own body temperature and instead relying on enhanced tolerance to adapt to environmental changes[4,5]. However, empirical evidence suggests that they can not only perceive ambient temperature fluctuations but also adapt to external changes through self-regulation[6]. Plants can accurately perceive environmental temperature, even responding strongly to minute changes[7]. For instance, a 1°C increase from 32°C to 33°C can strongly inhibit lettuce seed germination[8]. In addition, many plants can thermoregulate to maintain relatively stable tissue temperatures in the face of variable environmental temperatures. Some use variation in leaf functional traits to

thermoregulate and avoid unfavorable temperature extremes[9]. Others create metabolic heat to thermoregulate and attract pollinators or increase growth rates[10].

Despite this diverse and scattered literature, the implications of thermoregulation have been difficult to implement. Many studies in physiology, ecology, and climate science still regard plants as poikilotherms, with temperatures that are determined solely by the environment[11]. A. Savvides et al demonstrated a limited homeothermy of apical bud meristems using thermocouples[12]. Michaletz et al used a cellulose δ18O model parameterized with data for climate and wood cellulose δ18O to estimate the leaf temperatures, supporting limited homeothermy in leaves across temperature and climate gradients[11,13], however, it is questioned as lack of the direct measurement of internal leaf temperature.

The existing plant temperature (T_{plant}) measurement technologies are very limited, thermocouple is invasive and its difficult for measuring the temperature of thin leaves. The infrared thermography mainly measures the surface temperature of plant bodies and is greatly affected by the environment and range[14,15]. Fluorescent probes typically rely on their temperature-dependent luminescent properties for in vivo temperature measurement, offering the benefits of non-invasive and sub-micrometer scale[16-18]. However, conventional fluorescent probes are not suitable for detecting the T_{plant} due to the inherent barrier effects of cell walls[19], the interference of the complex and dynamic biochemical environment within plant tissues[20], especially when air temperature (T_{air}) changes[21], and as well as background noise from autofluorescence[22].

Here, using lab-made nano-thermal sensors and time-gated imaging technology, we have achieved, for the first time, the reliable and accurate measurement of subcellular-level temperature response within plants. Our findings reveal that the internal temperature is significantly different from the ambient temperature. We discovered a multilevel temperature regulation system where plants exhibit two-phase responses to temperature stress: an initial response phase and a steady-state phase. Within *N.benthamiana* leaves, upon a change in T_{air} of approximately 20°C (increased to 45°C from 24°C or decreased to 5°C from 24°C), the homeostasis of internal plant temperature was reestablished with a thermal gradient, decreasing progressively from the cell wall ($\Delta T_{cw} \approx$ 10°C) to the cytoplasm ($\Delta T_{cyt} \approx$ 7°C), while remaining nearly constant in chloroplasts ($\Delta T_{chl} \approx$ 1°C). This thermoregulation was consistent across *N.benthamiana*, *Arabidopsis*, and tomato, demonstrating plants' universal capability to maintain thermal homeostasis through sophisticated regulation. These results uncover active, compartment-specific thermal homeostasis in plants, challenging the classical view of poikilothermy and providing a framework for understanding metabolic stability under fluctuating temperatures.

Results

Construction of an internal temperature detection system for plants

To investigate how plants regulate their internal temperature, we developed a non-invasive approach for real-time temperature monitoring at subcellular resolution based on the long lifetime nano-thermal sensors (p-AuNPs) and time gated imaging system, as shown in the Fig.1.

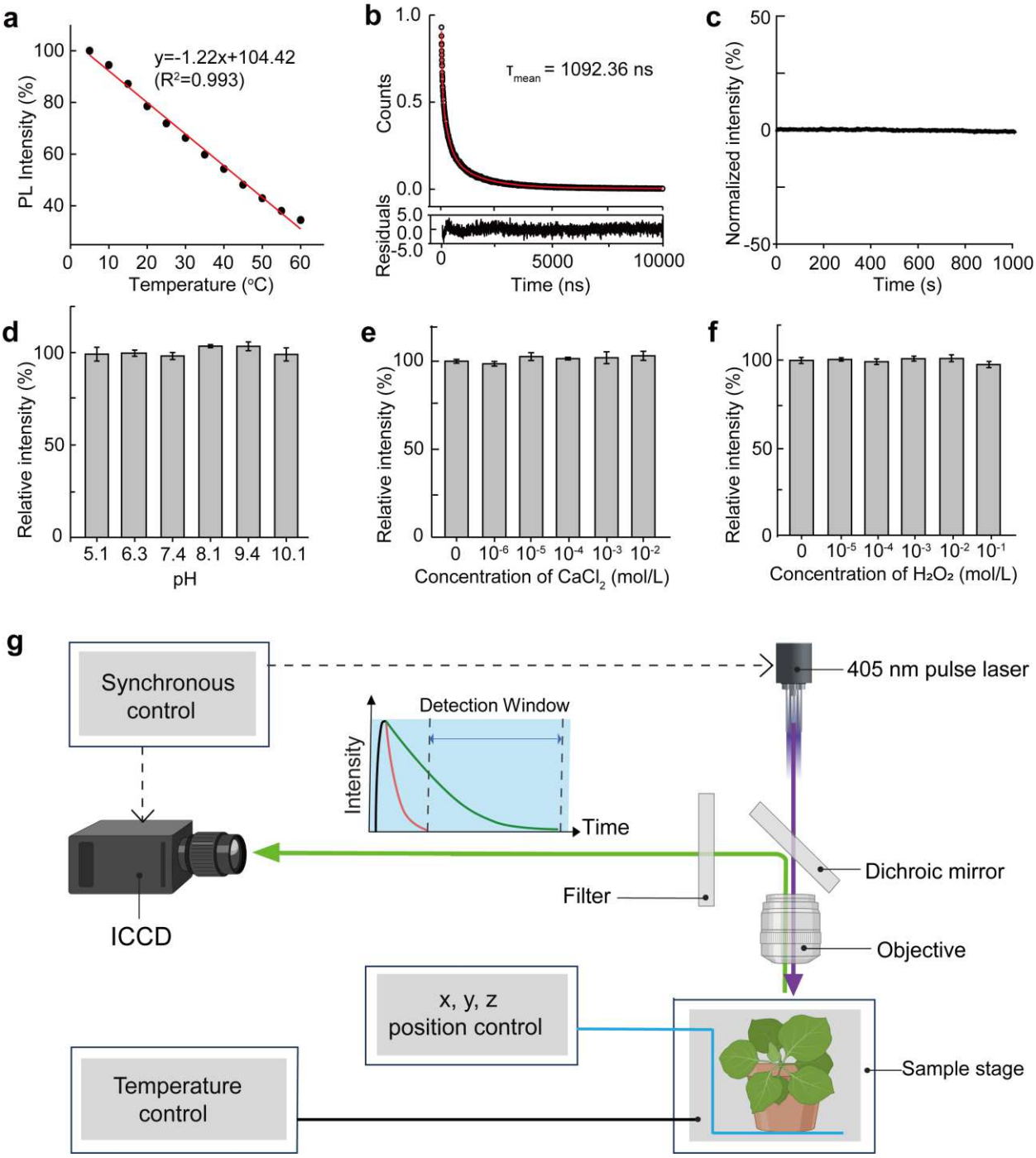

Fig.1 | A schematic diagram of plants temperature detection. a, The dependence of photoluminescence (PL) from p-AuNP@HTT on temperature ranging from 5°C to 60°C. The fluorescence intensity changes linearly with temperature, decreasing by 1.22% for every 1°C increase in temperature. **b**, The fluorescence lifetime of p-AuNPs at 25°C. **c**, T photostability of p-AuNPs determined by a time-gated imaging system, with a time delay of 100 ns ($\lambda_{excitation}$ = 405 nm). **d**, The relative PL intensity of p-AuNPs vs pH values. **e**, The relative PL intensity of p-AuNPs vs Ca^{2+} concentration. **f**, The relative PL intensity of p-AuNPs vs H_2O_2 concentration. The error bars represent the standard deviations obtained from three parallel experiments. **g**, Schematic diagram of measurement of the internal temperature of plants. The detection system mainly consists of the following modules: a ICCD for fluorescence signal acquisition, temperature

control unit, x/y/z position control system, and an excitation light source of 405 nm pulse laser. By using time-gated technology and long lifetime p-AuNPs, the autofluorescence of leaves and excitation background noise can be effectively removed, enabling accurate detection of the internal temperature of plants.

The temperature-sensitive nanoprobes, polymer-encapsulated photoluminescent gold nanoparticles (p-AuNPs) was prepared through a two-step process: photochemical synthesis of L-AuNP@HTT followed by PMMA-co-MMA coating for enhanced stability. As shown in Fig. 1a, these nanoprobes exhibit excellent temperature-dependence in the range from 5°C to 60°C, remarkable stability across physiologically relevant conditions, maintaining consistent photoluminescence intensity over a wide pH (pH = 5.0-10.0) and H_2O_2 concentration range (Fig. 1d, 1f), and under varying ionic conditions including Ca^{2+} (0-10^{-2} mol/L) (Fig. 1e), K^+, Na^+, and Mg^{2+} (Fig. S2). This exceptional stability ensures reliable temperature measurements against dynamic fluctuations in the plant's complex and intricate biochemical environment. Moreover, these p-AuNPs exhibit a long luminescence lifetime (~1000 ns) (Fig. 1b), far exceeding the typical plant autofluorescence (< 20 ns[23]), which allows effective suppression of background signals and ensures accurate detection of the temperature-sensitive probe. When combined with time-gated imaging[24,25], this feature is crucial for reliable internal plant temperatures (T_{plant}) measurements (see Methods for details).

The AuNPs were infiltrated into plant leaves through the abaxial surface of the leaf with a needleless syringe, and cultured in the temperature-controlled chamber for 5-6 hours, which ensures the sensors were delivered and stably labelled to the leaf tissues. Multiple plant species, including *N.benthamiana*, *Arabidopsis*, and tomato were employed in this study. The p-AuNPs were not only distributed in the veins, stomas, the cell walls of leaf cells, but also in the chloroplasts of guard cells and cytoplasm (Fig. S5). The widespread distribution of the nanoparticles and their ability to enter cells enable simultaneous monitoring of temperature responses across different plant compartments at subcellular resolution.

A detection area far from the infiltration site was selected to ensure the signals are sent from those sensors inside the leaf. A 405 nm picosecond laser was used as excitation source, and the fluorescence signals were collected using a time-gated intensified CCD (ICCD). With a 100 ns gate delay, the leaf autofluorescence could be eliminated, as shown in Figure S6. Air temperature was monitored with a mini thermocouple located near the detection spot, and a position control system was designed to prevent the shift of sample caused by the change of temperature.

Temperature response and regulation in *N.benthamiana* leaves

We systematically examined temperature dynamics within *N.benthamiana* leaves under both cold and heat stress. As a baseline, ambient temperature was first maintained constant at 24°C for approximately 200 seconds (Fig. 2a, 2c). During this period, both the air temperature (black diamonds) and the relative photoluminescence intensity of p-AuNPs (blue and red lines) remained stable, confirming the reliability of our detection system.

Under the cold stress, when air temperature was subsequently decreased from 24°C to 5°C, we

observed a distinct two-stage response in leaf internal temperature. During the initial stage, the photoluminescence intensity increased linearly as air temperature dropped from 24°C to approximately 13°C (Fig. 2b), indicating a corresponding decline in leaf temperature. The decrease of temperature of the cell wall ($\Delta T_{cw} \approx 5$°C) is much less than that of air temperature ($\Delta T_{air} \approx 12$°C), suggesting a corresponding regulation in leaf was triggered. We named this stage as the response phase (RP). Notably, when air temperature furthering cooling below 13°C, the photoluminescence intensity plateaued despite ongoing environmental cooling, which indicates the internal temperature has reached a steady-state phase (SSP) after regulation in RP.

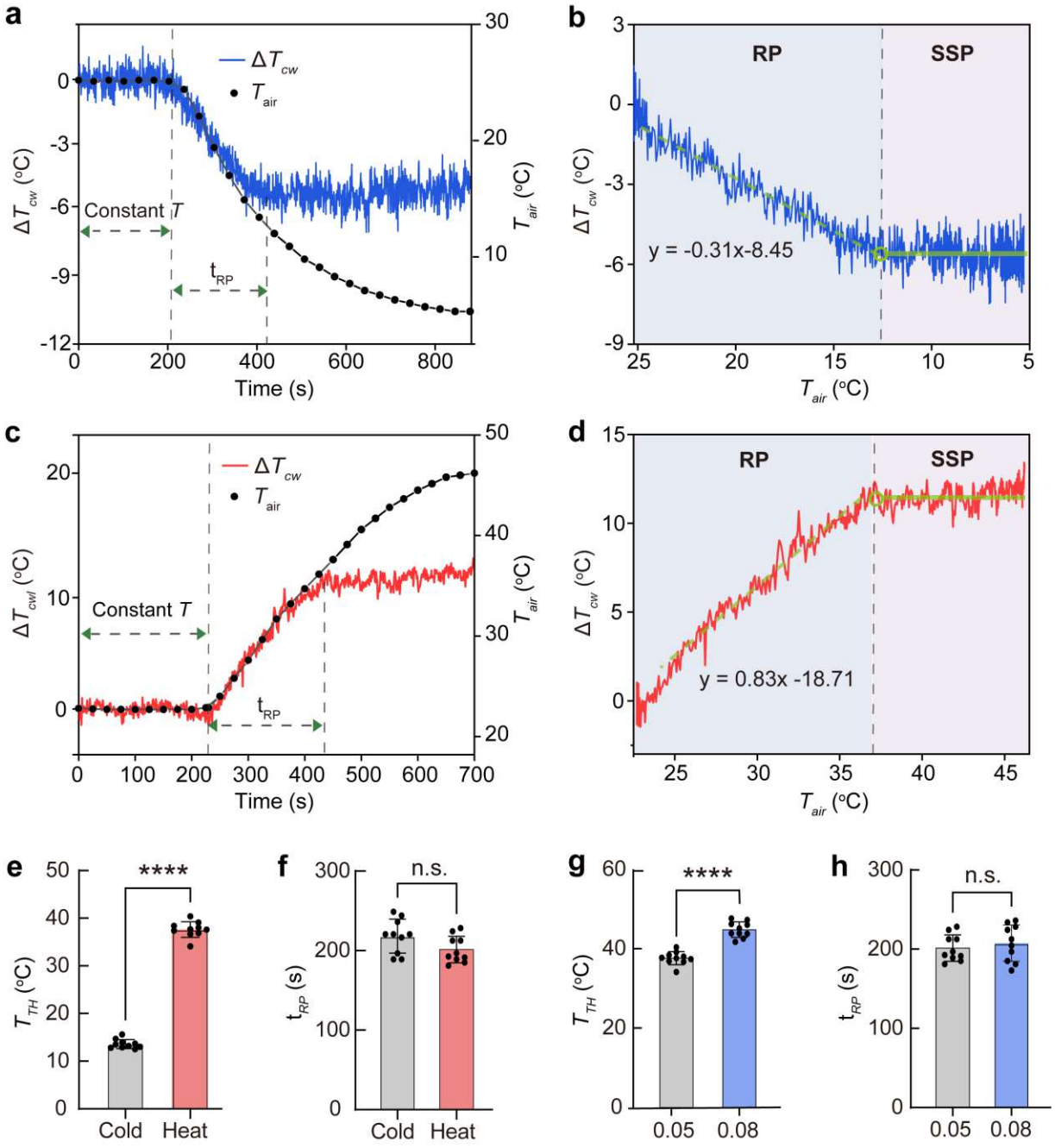

Fig.2 | Temperature response and regulation in *N.benthamiana* leaves. a, Temperature change (ΔT) in the cell wall of *N.benthamiana* leaves and ambient temperature variation over time under cold stress. **b**, The

change of leaf temperature vs air temperature during cold stress. Two phases, the response phase (RP) and the steady-state phase (SSP) could be observed. During RP, the internal leaf temperature changes with environmental temperature, whereas during SSP, the internal leaf temperature tends to be stabilized despite changing environmental temperature. **c**, Temperature change (ΔT) in the cell wall of *N.benthamiana* leaves and ambient temperature variation over time under heat stress. **d**, The leaf temperature change vs air temperature during heat stress. Similarly, two distinctly different phases (RP and SSP) could be observed. The temperature threshold (T_{TH}) at transition points between RP and SSP was indicated with a green circle. **e**, Comparison of T_{TH} under cold and heat stress. It was 13.4 ± 1.2°C under cold stress and 37.2°C ± 1.9°C under heat stress. **f**, Comparison of RP time (t_{RP}) between cold and heat stress (218 ± 21 s for cold stress; 201 ± 17 s for heat stress); **g**, Comparison of T_{TH} under different heating rates (37.2 ± 1.9°C for 0.05°C/s and 44.7 ± 1.9°C for 0.08°C/s). **h**, Comparison of RP under different heating rates (201 ± 17 s for 0.05°C/s; 208 ± 23 s for 0.08°C/s). The symbols ΔT_{cw} represent the temperature of cell wall. Two-tailed Student's *t*-test for comparison. $n = 10$. ****$p < 0.0001$; *n.s.*: no significant difference.

A parallel pattern was observed during heat stress experiments. After an initial constant temperature period at approximately 24°C, increasing air temperature induced a similar two-phase response (Fig. 2c). During the RP, leaf temperature increased linearly with air temperature until reaching approximately 37°C, at which point it enter the SSP and maintained stable internal temperature despite continued environmental heating (Fig. 2d). The increase of temperature inside plant is also much less than that of air temperature. The two SSP stages of cooling and heating proved the plants were capable of maintaining thermostatic to some extent under temperature stress.

The temperature threshold (T_{TH}) at transition points between RP and SSP occurred at 13.4°C ± 1.2°C under cold stress and 37.2°C ± 1.9°C under heat stress (Fig. 2e), the duration of the RP (t_{RP}) phase was approximately 200 seconds under both cold and heat conditions (Fig. 2f). To investigate whether this temporal parameter represents an inherent property of the temperature regulation system, we examined the responses under different heating rates. Increasing the average heating rate from 0.05°C s^{-1} to 0.08°C s^{-1} under the same overall temperature change (ΔT_{air} = 23°C, from 24°C to 47°C), we observed no significant difference in t_{RP} (Fig. 2g, h). However, the faster heating rate resulted in a higher stabilization temperature (T_{TH} = 44.7°C), suggesting that while the temporal dynamics of temperature regulation are conserved, the absolute temperature thresholds of SSP can be modulated by the rate of environmental temperature change.

We examined temperature responses in *N.benthamiana* leaf grinding solution. Notably, under identical temperature stress conditions, no SSP was observed in the leaf grinding solution (fig. S8), instead, the temperature of the grinding solution changed proportionally with environmental temperature. The lack of temperature stabilization in disrupted tissue indicates that thermal homeostasis may depends on coordinated regulation within intact cells or tissues, rather than on isolated cellular components.

Additionally, we discovered that leaf developmental stage significantly influenced thermal regulation capacity. Under the same temperature stress conditions, 2-week-old leaves demonstrated faster adaptation to temperature changes, reaching internal temperature stability more rapidly than 4-week-old leaves (Fig. S9). This suggests that plants at different growth stages have different regulate abilities to temperature stress.

Multi-level temperature regulation within *N.benthamiana* leaves

The p-AuNPs were distributed across different cell compartments in the *N.benthamiana* leaves, including the cell wall, cytoplasm, and chloroplasts (Fig. S5). When comparing temperature variations across these compartments in response to air temperature changes (ΔT_{air}), we discovered a striking gradient of temperature regulation (Fig. 3). The measured temperature responses of different cellular compartments showed distinct patterns when plotted against ΔT_{air}. All compartments exhibited temperature changes that significantly deviated from the theoretical 1:1 line (dotted line), which would represent passive temperature following caused by thermal conduction without regulation. The deviation increased progressively from the cell wall to the chloroplasts, with the chloroplasts (green lines) showing the smallest response to air temperature changes, followed by the cytoplasm (yellow lines), the cell wall (blue lines), and the stomata (red lines), which exhibited the largest response.

During cold stress ($\Delta T_{air} \approx 20$°C, from 24°C to 5°C), chloroplasts maintained remarkably stable temperature, changing by only 1.3°C (ΔT_{chl}). The cytoplasm showed moderate temperature variation (ΔT_{cyt} = 3.7°C), while the cell wall exhibited larger changes (ΔT_{cw} = 7.1°C). Notably, even the stomata, which are directly exposed to external air, showed regulated temperature changes (ΔT_{stoma} = 9.0°C), significantly lower than the air temperature change (Fig. 3b, d).

Similarly, under heat stress ($\Delta T_{air} \approx 20$°C, from 24°C to 45°C), we observed a consistent hierarchy of differential regulation: chloroplasts temperature increased by only 0.2°C, cytoplasmic temperature by 6.9°C, and cell wall temperature by 9.2°C, while stomatal temperature showed the largest change of 15.0°C (Fig. 3a, c).

This pattern ($\Delta T_{air} > \Delta T_{stoma} > \Delta T_{cw} > \Delta T_{cyt} > \Delta T_{chl}$) demonstrates a sophisticated multi-level temperature regulation system within plants. Under heat stress, the first level of regulation occurs outside the cell, where stands a temperature difference of approximately 12°C from the external environment (ΔT_{cw} = 9.3°C vs $\Delta T_{air} \approx 20$°C). The signal sent from the p-AuNPs labelled on the cell wall likely represents the temperature of micro environment outside the cell, which could be modulated by the evaporative cooling effect. The transpiration provides initial temperature buffering through water evaporation. This is consistent with that the approximately 7°C difference between stomata (ΔT_{stoma} = 15.0°C) and air temperature changes ($\Delta T_{air} \approx 20$°C), considering the stomata are directly exposed to the air. The second level regulation originate from the 2.6°C difference between the temperature change of the cell wall and cytoplasm (ΔT_{cw} - ΔT_{cyt}). This is likely mediated by the transmembrane regulation together with the dynamic biochemical processes in cytoplasm. This serves as a thermal barrier with its complex matrix structure. The third level regulation exists between cytoplasm and organelles, especially for chloroplasts. It stands a remarkable 6.7°C temperature difference between the cytoplasm and chloroplast. The regulation ensures the chloroplasts maintaining the most stable temperature, protecting these essential photosynthetic organelles from thermal fluctuations.

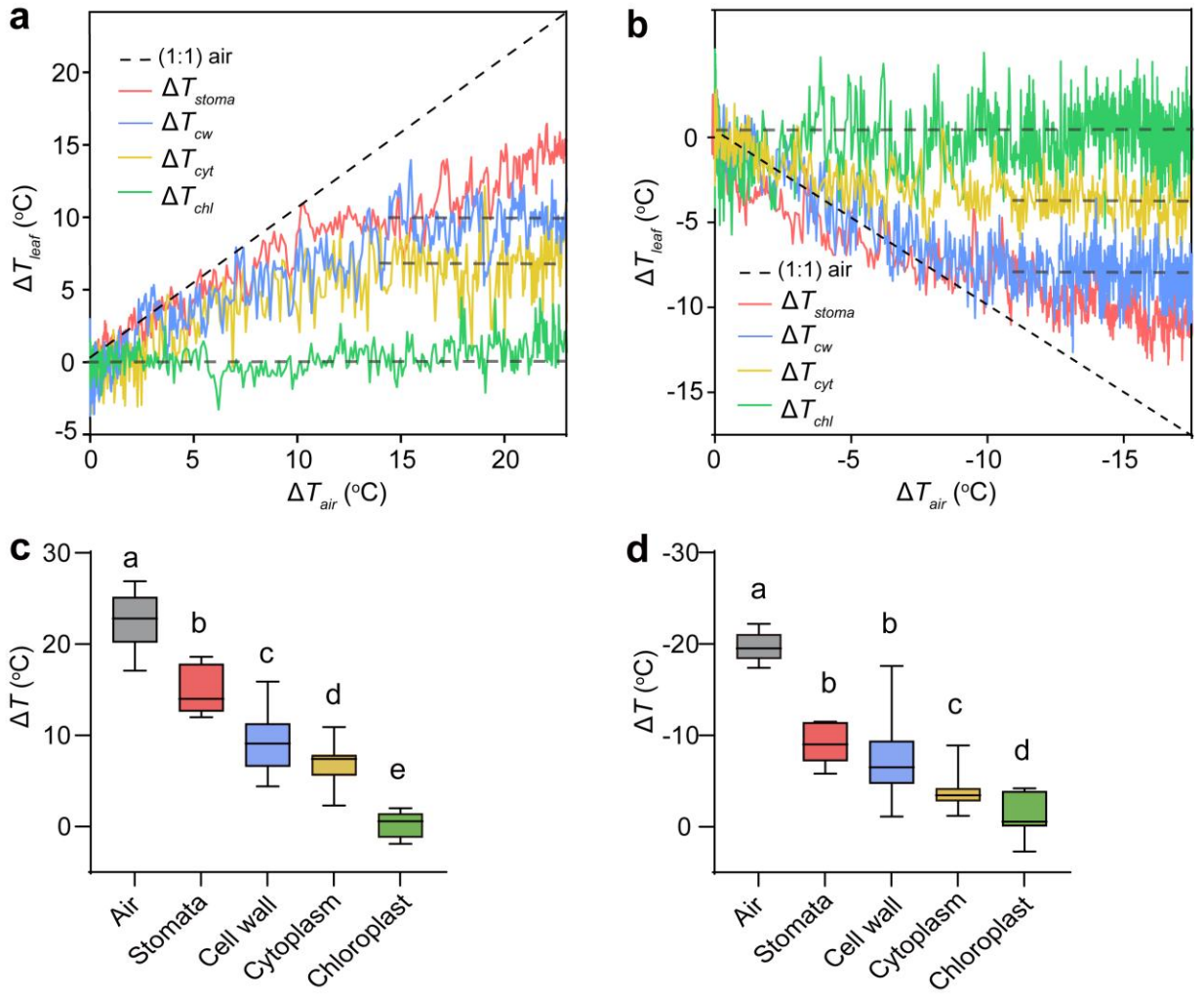

Fig.3 | Multi-level temperature regulation within *N.benthamiana* leaves reveals subcellular thermal gradients. **a-b**, Typical response curves of temperature changes in stomata (stoma: red line), cell wall (cw: blue line), cytoplasm (cyt: yellow line) and guard cell chloroplasts (chl: green line) as a function of air temperature change under heat stress (a) and cold stress (b) The dashed diagonal line has a slope of 1:1, representing the temperature response of poikilothermic organisms with no thermoregulation ability. Air temperature change (ΔT_{air}) is defined as $T_0 - T_i$; temperature change in different cellular compartments (ΔT_{leaf}) is calculated as $(I_0 - I_i) \times 100 / 1.23$. **c**, Comparison of ΔT among different plant cellular compartments vs ΔT_{air} during heat stress ($\Delta T_{air} \approx 20$°C, $\Delta T_{stoma} = 15.0 \pm 2.4$°C, $\Delta T_{cw} = 9.3 \pm 3.1$°C, $\Delta T_{cyt} = 6.9 \pm 2.2$°C, $\Delta T_{chl} = 0.2 \pm 1.5$°C). **d**, Comparison of ΔT among different compartments vs ΔT_{air} during cold stress ($\Delta T_{air} \approx 20$°C, $\Delta T_{stoma} = 9.0 \pm 2.8$°C, $\Delta T_{cw} = 7.1 \pm 3.4$°C, $\Delta T_{cyt} = 3.7 \pm 2.4$°C, $\Delta T_{chl} = 1.3 \pm 1.9$°C). Temperature changes in different compartments show a gradient distribution from outer to inner layers ($\Delta T_{air} > \Delta T_{stoma} > \Delta T_{cw} > \Delta T_{cyt} > \Delta T_{chl}$). Different lowercase letters indicate significant differences ($p < 0.05$, one-way analysis of variance with Tukey's post hoc test).

Thermoregulation among different plant species

We extended our study to *Arabidopsis* and tomato, comparing their responses with those of *N.benthamiana*. All three species exhibited the characteristic two-phase temperature response pattern (RP and SSP phases) under both cold and heat stress conditions, as shown in Fig. 4a and 4b. All three species demonstrated comparable temperature regulation efficiency, with internal

temperature changes significantly smaller than environmental variations (Fig S10-11). These results revealed that these temperature regulation patterns represent a conserved feature across diverse plant species.

Under cold stress, the RP duration (t_{RP}) to reach steady state was 218.2 ± 21.4 seconds for *N.benthamiana*, 209.2 ± 29.4 seconds for *Arabidopsis*, and 242.5 ± 25.1 seconds for tomato (Fig. 4b). And t_{RP} for each specie keep constant under various temperature change rate. The temperature point T_{TH} at which leaves transitioned from RP to SSP phase was 13.4 ± 1.2°C for *N.benthamiana*, 15.1 ± 1.6°C for *Arabidopsis*, and 13.0 ± 1.6°C for tomato at the same temperature decrease rate of 0.025°C s^{-1} (Fig. 4c). The difference of t_{RP} among species may reflects their genetic variations of the capability responding to the air temperature change.

Similarly, under heat stress, t_{RP} also displayed difference across species: 213.2 ± 22.8 seconds for *N.benthamiana*, 187.9 ± 19.3 seconds for *Arabidopsis*, and 194.9 ± 20.2 seconds for tomato (Fig. 4e). Species-specific transition points T_{TH} were observed at 44.7 ± 1.9°C for *N.benthamiana*, 41.0 ± 2.1°C for *Arabidopsis*, and 40.2 ± 2.7°C for tomato (Fig. 4d) under a heating rate of 0.08°C/s. These transition temperatures correspond well with known physiological thresholds for photosynthetic function, suggesting coordination between temperature regulation and metabolic requirements. All species exhibited robust temperature regulation, maintaining internal temperature changes substantially below air temperature variations (Fig. 4h), consistent with previous observations of leaf temperature decoupling from air temperature[23].

These findings suggest that the capacity for temperature homeostasis is widely conserved across diverse plant species. When air temperature changed by approximately 20°C during cold stress, internal temperature changes were limited to $\Delta T_{N.benth}$ = 5.4 ± 1.4°C, ΔT_{tomato} = 4.8 ± 1.3°C, and $\Delta T_{Arabidopsis}$ = 4.1 ± 1.6°C. Under heat stress ($\Delta T_{air} \approx 25$°C), similar regulation was observed: $\Delta T_{N.benth}$ = 10.6 ± 2.6°C, ΔT_{tomato} = 9.7 ± 1.8°C, and $\Delta T_{Arabidopsis}$ = 8.4 ± 2.3°C. This regulated response aligns with theoretical predictions of leaf energy balance[11,24] and supports the concept that plants actively maintain their temperature within optimal ranges for physiological processes[25,26]. The consistency of these responses across species suggests that temperature homeostasis represents a fundamental adaptation in plant biology, likely emerging early in plant evolution to enable stable performance under varying environmental conditions[24].

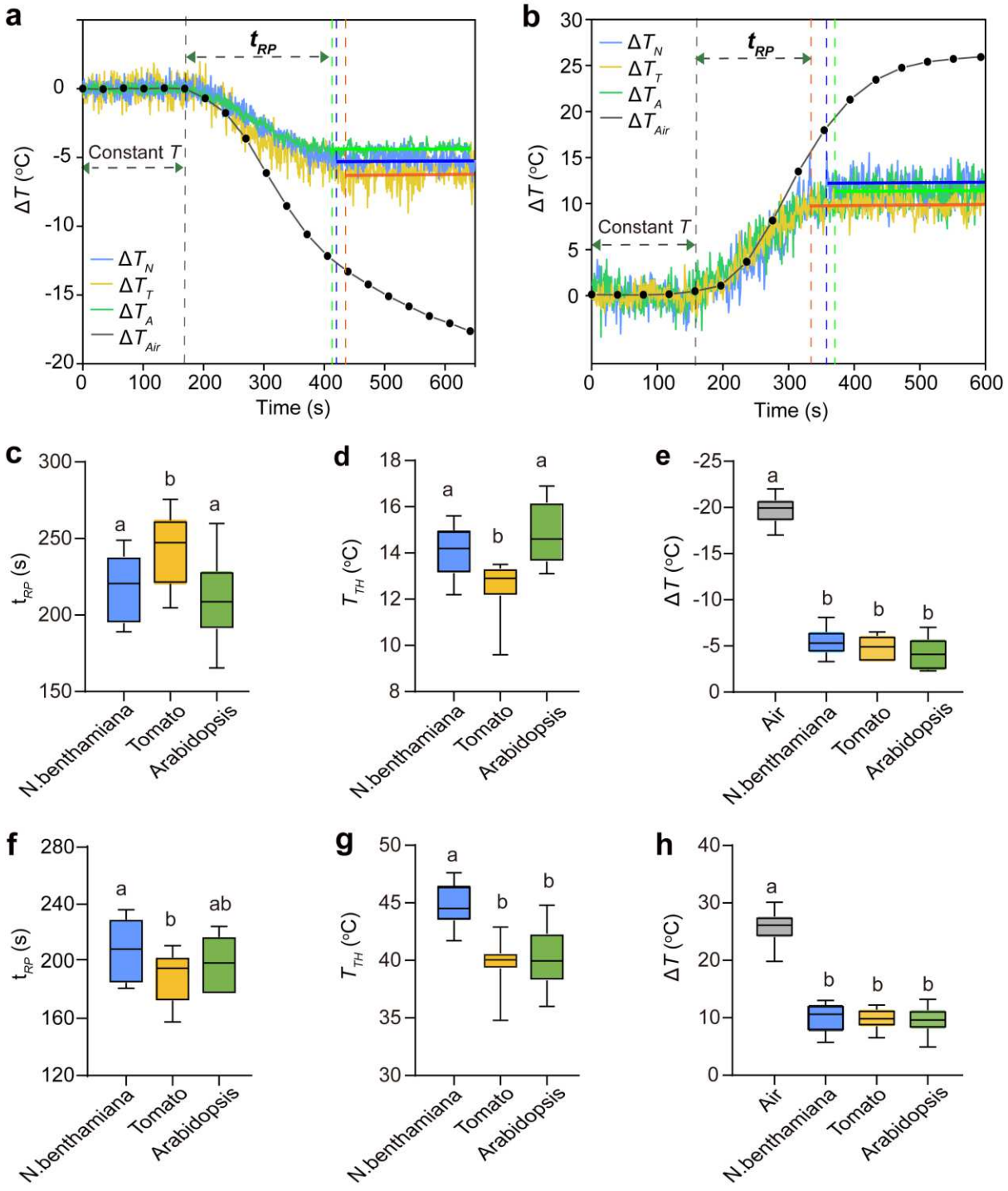

Fig.4 | Comparative analysis of temperature regulation across three plant species under cold and heat stress. a, The typical curves of ΔT_{leaf} and ΔT_{air} as a function of time in leaves of three plant species under cold stress. **b**, The typical curves of ΔT_{leaf} and ΔT_{air} as a function of time under heat stress. The black dots indicate the air temperature measured by a thermocouple sensor, the blue line indicates the ΔT in *N.benthamiana* leaves (ΔT_N), the yellow line indicates the ΔT of tomato leaves (ΔT_T), and the green line indicates the ΔT of *Arabidopsis* leaves (ΔT_A). t_{RP} is the durations of the RP phase. **c**, Comparison of the t_{RP} in three plant species under cold stress (t_{RPN}: 218.2 ± 21.4 s, t_{RPT}: 242.5 ± 25.1 s, t_{RPA}: 209.2 ± 29.4 s). **d**,

Comparison of the temperature threshold (T_{TH}) at transition points between RP and SSP phases occurred under the cold stress in three plant species (T_{THN} = 13.4 ± 1.2°C, T_{THT} = 13.0 ± 1.6°C, T_{THA} = 15.1 ± 1.6°C). **e**, The comparison of ΔT in different plants leaves under cold stress ($\Delta T_{air} \approx 20$°C, ΔT_N = 5.4 ± 1.4°C, ΔT_T = 4.8 ± 1.3°C, ΔT_A = 4.1 ± 1.6°C). **f**, Comparison of the t_{RP} in different plants under heat stress (t_{RPN}: 213.2 ± 22.8 s, t_{RPT}: 197.9 ± 20.2 s, t_{RPA}: 187.9 ± 19.3 s). **g**, Comparison of the temperature threshold (T_{TH}) at transition points between RP and SSP phases occurred under the heat stress in three plant species (T_{THN} = 44.7 ± 1.9°C, T_{THT} = 40.2 ± 2.7°C, T_{THA} = 41.0 ± 2.1°C). **h**, The comparison of ΔT in different plants leaves under heat stress ($\Delta T_{air} \approx 25$°C, ΔT_N = 10.6 ± 2.6°C, ΔT_T = 9.7 ± 1.8°C, ΔT_A = 8.4 ± 2.3°C). n = 10; Different lowercase letters indicate significant differences ($p < 0.05$, one-way analysis of variance with Tukey's post hoc test).

Water channel regulation model and simulation

When plants encounter environmental temperature stress, they can trigger a series of regulatory mechanisms to adapt to temperature fluctuations. Generally, the plant temperature regulation mechanisms can be categorized into passive and active regulation. Passive regulation primarily involves temperature receptors that activate signaling pathways to enhance the plant's tolerance to external temperature changes, thereby promoting acclimation processes such as cold- or heat-induced morphogenesis (thermomorphogenesis)[27,28]. This is typically a slow and prolonged process. Active regulation, on the other hand, primarily involves transpiration and the intensity of life processes (such as photosynthesis and metabolic processes) to control heat exchange and generation. As one of the most important organs in plants, leaves play a very important role in regulating plant temperature. Traditionally, due to the thinness of leaves, they are often treated as thermally homogeneous bodies, assuming that the temperature is uniform throughout the interior and equal to the surface temperature[9,24]. However, our experimental results reveal for the first time that temperature distribution varies significantly across different parts within a plant leaf, suggesting the existence of a complex mechanism for temperature regulation.

In plant leaves, water is the most abundant substance and possesses the highest heat capacity[29]. Consequently, the change of water plays a crucial role in regulating temperature inside plant leaf across different regions[30]. Due to the presence of biological membranes, water in the leaf is compartmentalized into distinct units, such as the apoplast, cytoplasm, and various organelles. Heat exchange between these units occurs primarily through thermal conduction, thermal convection, and phase transitions (e.g., latent heat in transpiration). Water flows between these units through specific channels and is regulated by thermal sensing systems, thereby facilitating heat exchange and temperature control[31]. Besides thermal conduction, the apoplast dissipates heat via transpiration through stomata[32]; Water exchange between the intracellular and extracellular environments occurs via aquaporins on the plasma membrane, while exchange between organelles and the cytoplasm occurs through channels on the organelle membranes[31]. Due to metabolic heat generation and varying pathways of heat diffusion, temperature differences arise among these parts. When the ambient temperature is constant, water exchange between different units leads to a dynamic equilibrium of heat, achieving thermal homeostasis. We propose a water-channel model for temperature regulation, as shown in Figure 5a, which includes transpiration channels, plasma

membrane water channels, and organelle membrane water channels.

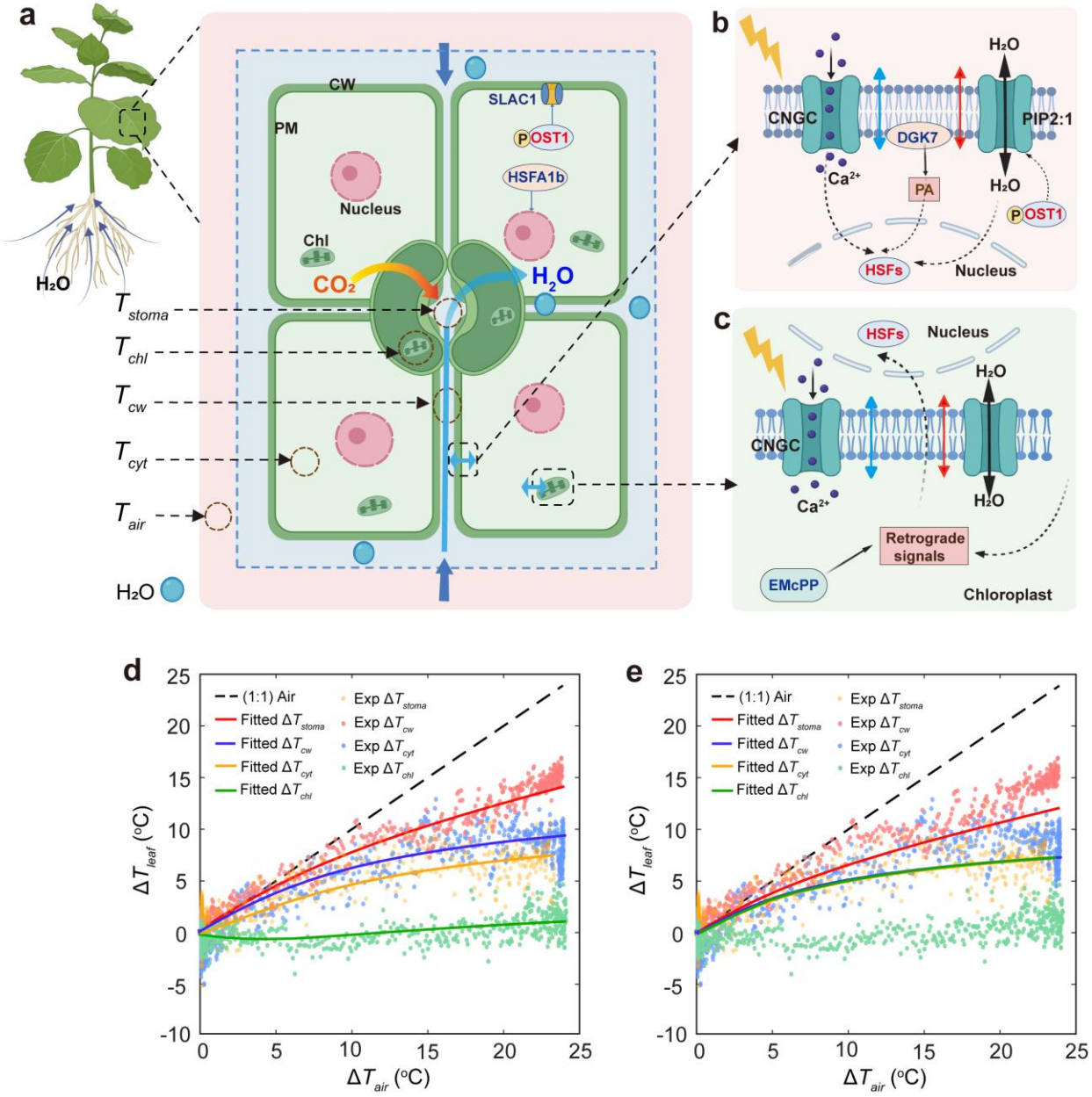

Fig.5 | Schematic model of multilevel thermoregulation in plant cells. a, **b**, and **c** indicate schematic models of multiple water channels in a plant leaf and the regulations of the channels. Under temperature stress, the thermal sensors (HSFA1b) rapidly activate modulation system (OST1) and adjust the stomatal opening and closing, regulate leaf transpiration; and activate the aquaporin PIP2;1, thereby modulate water permeability of membrane. The symbols T_{air}, T_{stoma}, T_{cw}, T_{cyt} and T_{chl} represent the temperature of air, stomata, cell wall, cytoplasm, and chloroplast respectively; **d**, The solid curves show the simulation results of temperature changes according to equation 1, 2, and 3, which are well consistent with our experimental data shown in Fig.3; **e**, The simulation results when the water channels on membrane are blocked, which indicates the internal temperature gradients are eliminated.

The water in the apoplast is freely mobile, so its temperature can be considered equivalent to the cell wall temperature (T_{cw}). Its temperature variation is regulated primarily through heat

changes via three pathways: thermal conduction between the leaf surface and the apoplast; the latent heat of vaporization as water in the apoplast vaporizes and transpires through stomata; and heat exchange across the plasma membrane (including heat conduction and transmembrane transport of water with different temperatures). When the ambient temperature is constant, the heat exchange reaches a dynamic equilibrium, and the apoplastic temperature remains constant, as shown in the initial phase of Figure 3. Conversely, when the environment changes steadily, thermal sensors in the leaf (e.g., HSFA1b) are activated. These regulate stomatal conductance by modulating OST1 expression to control leaf transpiration and activate aquaporin PIP2;1 to modulate plasma membrane permeability, thereby regulating water exchange and heat transfer between the apoplast and cells[31,33]. When this adjustment counteracts the internal temperature changes induced by environmental fluctuations, heat exchange reaches a new equilibrium, and the apoplastic temperature achieves a new steady state, as depicted in Figure 3. The apoplast accounts for most of water transport and plays a dominant role in regulating internal leaf temperature, providing a relatively stable microenvironment for leaf cells. The temperature variation in the apoplast can be expressed by Equation 1, and the details of the theoretical simulation are provided in the Supplementary Materials (S12).

$$C\frac{dT_{apo}}{dt} = H_{s-apo} + H_{apo-cyt} \quad (1)$$

Where $H_{s-apo} = hA_{s-apo}\left(T_s - T_{apo}\right) - Q_t$ is the heat exchange between apoplast and leaf surface, the first term $hA_{s-apo}\left(T_s - T_{apo}\right)$ indicates the thermal conduction between apoplast and leaf surface, and second term Q_t is the latent of transpiration; $H_{apo-cyt} = hA_{apo-cyt}\left(T_{apo} - T_{cyt}\right) - Q_{apo-cyt}$ is the heat exchange between apoplast and cytoplasm, the first term is thermal conduction, and second one is thermal convection via water channels on plasma membrane.

The apoplast provides a microenvironment for the cells. The establishment of its thermal homeostasis lays the foundation for the thermal homeostasis of the cytoplasm and organelles. The temperature variation of the cytoplasm is determined by heat transfer across the cell boundary, convective water flow across the plasma membrane, energy exchange between the cytoplasm and subcellular units (such as nucleus and organelles), and heat generated by intracellular life activities (including metabolic heat release, work done by transport and synthesis, and phase changes of matter). The heat variation is described by Equation 2. To simplify the model, Equation 2 equates the nucleus and various organelles besides chloroplasts to a single equivalent heat source.

$$C_{cyt}\frac{dT_{cyt}}{dt} = H_{apo-cyt} + G_{cyt} + H_{cyt-org} \quad (2)$$

Here G_{cyt} is heat generation in cytoplasm caused by life activities, and $H_{cyt-org} = hA_{cy-chl}\left(T_{cyt} - T_{chl}\right) - Q_{chl} + hA_{cy-other}\left(T_{cyt} - T_{other}\right) - Q_{other}$ is the heat exchange between cytoplasm and organelles (including chloroplasts and others). First term indicates thermal conduction, second term Q_{chl} indicates the heat convection between cytoplasm and chloroplasts.

Similarly, the heat and temperature within organelles, such as chloroplasts, are described by Equation 3.

$$C_{chl}\frac{dT_{chl}}{dt} = hA_{cyt-chl}\left(T_{cyt} - T_{chl}\right) - Q_{chl} + G_{chl} \quad (3)$$

Here G_{chl} is the heat generation caused by life activities in chloroplasts.

The results of the theoretical simulation are shown in Figures 5d and 5e.

The results of the theoretical simulation are shown in Figures 5d and 5e. Fig. 5d demonstrates that the water channel model fits the experimental results well. Interestingly, when the ambient temperature is at the initial level (≈ 24°C), the simulation indicates that the initial temperatures at the stomata, apoplast, cytoplasm, and chloroplasts are 24.1°C, 24.2°C, 26.7°C, and 35.9°C respectively, specifically following the order of $T_{cw0} < T_{cyt0} < T_{chl0}$, $T_{sto0} \approx T_{s0}$. These results suggest that plants exhibit a temperature gradient internally, where the intracellular temperature is higher than the extracellular temperature; notably, the temperature of chloroplasts can reach approximately 37°C.

When the ambient temperature rises, the apoplastic temperature increases accordingly. However it begins to maintain a constant temperature of 37.2°C. Even when the ambient temperature is as high as 45°C, the plant leaf can maintain the apoplast at a relative lower level through transpiration, thereby providing a suitable microenvironment for cellular activities. Although the intracellular temperature also rises correspondingly, the overall gradient distribution remains unchanged. Heat generated by life activities within the cell is consistently dissipated via the apoplastic transpiration pathway. The critical cellular sites, such as chloroplasts, can still maintain the conditions necessary for life activities.

The results in Figure 5e further reveal that water channels on the plasma membrane and organelle membranes are crucial for maintaining the temperature gradient within the cell. When these membrane channels are disabled (setting their conductance to zero), although thermal conduction between different parts of the leaf persists, the internal temperature gradient disappears, and the temperatures of all intracellular components converge with the apoplastic temperature. This indicates that water channels on biological membranes are essential and indispensable for maintaining the thermal environment required for intracellular life activities.

Discussion

It is generally believed that the enhanced adaptation resulting from thermomorphogenesis is the primary pathway when plants face temperature stress. For instance, at air temperatures of 25-30°C, phytochrome B (phyB) in *Arabidopsis* seedlings undergoes a conformational shift within the nucleus, transitioning from the biologically active Pfr:Pfr homodimer to the inactive Pr:Pr form. This temperature-dependent inactivation of phyB reduces its activity, suppresses the release of PIF4, and consequently promotes thermomorphogenesis[34]. TWA1 accumulates in nuclear subcompartments via phase separation, interacts with transcription factors JAM2 and TPL to form a repressor complex, and suppresses the expression of target genes[35]. the 5′UTR of PIF7 mRNA undergoes structural rearrangements that enhance PIF7 translation, which subsequently activates

downstream heat stress-responsive genes[36]. Collectively, these molecular sensors transduce thermal cues into coordinated biochemical responses, orchestrating multiple strategies to cope with temperature stress.

For a single leaf, the energy balance follows the law of conservation of energy, and can be expressed as Penman-Monteith equation[37,38]. It elucidates the dynamics of leaf surface temperature in response to environmental fluctuations, where the leaf was treated as heat homogeneous. Our work presents the first high-precision measurements of internal leaf temperature dynamics in plants, directly demonstrating active internal thermoregulation and the establishment of thermal homeostasis in plants. When plants are subjected to ambient temperature stress, their internal temperature is not as severe as one might expect. In fact, some critical regions even maintain a appropriate temperature consistently. When external temperatures fluctuate, whether increasing or decreasing, plants can maintain a stable internal temperature after a certain adjustment period. As shown in Figures 2 and 3, when ambient temperatures exceed specific thresholds ($T_{air} > T_{TH}$ = 37°C or $T_{air} < T_{TH}$ = 13°C), the internal temperature of the plant stabilizes and no longer changes with external variations. In other words, within a certain environmental range, plants exhibit thermostatic behavior. When environmental temperatures shift between 5°C and 45°C, the maximum internal temperature variation in plants is only 16.3°C, while the temperature change within chloroplasts is even smaller, less than 1.5°C. These results highlight not only exceptional thermal tolerance but also robust self-regulatory capacity, allowing plants to buffer vital organelles against rapid and extreme environmental changes, providing a new framework for understanding plant responses to temperature stress, what is supposed as water channel model.

The results of simulation show the temperatures at different locations within the plant leaf are different when plants live in a stable environment (24°C), and presents a gradient as $T_{cw0} < T_{cyt0} < T_{chl0}$, $T_{sto0} \approx T_{leaf}$. When ambient temperature changes, it activates temperature sensors inside plant, triggering multi-tiered active regulatory responses, such as adjusting stomatal conductance, regulate the aquaporin activity and plasma membrane permeability to modulate heat exchange, and potentially tuning metabolic activity to alter internal heat production[39-41]. These coordinated adjustments dampen, and eventually counteract, internal temperature fluctuations, ultimately re-establishing a new thermal equilibrium state.

Taking heat stress in *Arabidopsis* as an example, during the initial warming phase, rising T_{air} reduces outward (or increases inward) heat conduction efficiency, causing T_{cw} to increase. This rise activates temperature sensors such as HSFA1b, initiating internal regulatory programs—Under heat stress, the heat shock transcription factor HSFA1b is rapidly activated and translocated into the nucleus, where it directly binds to the promoter of OST1 and strongly induces its expression. As a central kinase, OST1 phosphorylates and activates downstream anion channels (SLAC1) in guard cells, and adjust the stomatal opening[42-44]. Under heat stress, increased stomatal aperture dramatically enhances leaf transpiration, which effectively lowers apoplastic temperature (T_{cw}). Because this regulatory response builds gradually, internal temperature initially rises with ambient temperature, so called RP phase in Fig.2b and 2d. A new thermal steady state i.e., SSP, is

established when heat accumulation from the environment equals heat loss via enhanced transpiration. Transpiration plays a crucial role in mitigating internal temperature fluctuations, buffering most of the external temperature variations. For instance, when ambient temperatures increase from approximately 24°C to 45°C, the temperature of apoplast changes by only 9.2°C, meaning nearly 13°C of the potential temperature increase is offset by this active regulatory process. This provides the cells with a relatively stable microenvironment for life processes, even under the extreme air temperature. Compared to the plant's thermomorphogenic process, this thermoregulatory response is rapid. The stomatal aperture significantly increases within 2~4 minutes[42-44], consistent with our measured RP duration ($t_{RP} \approx 3$ minutes). Different crop species exhibit variations in stomatal dynamics, and these differences in t_{RP} may serve as indicators of temperature adaptation capacity among plant species, as shown in Figure 4.

The change of temperature inside cytoplasm (ΔT_{cyt}) is largely determined by the thermal gradient between the extracellular compartment and the cytoplasm ($\Delta T_{cw} \rightarrow \Delta T_{cyt}$). Transpiration substantially attenuates heat stress from air temperature owing to the strong buffering effect, provides relative stable external microenvironment surrounding the cytoplasm. The influence on the cytoplasm caused by temperature change ΔT_{cw} is further diminished through several coordinated mechanisms, mainly by the heat exchange via water channels.

Under high temperature conditions, the influx of Ca^{2+} and other solutes may increase cellular osmotic pressure[45,46], which could potentially enable OST1 to activate the aquaporin PIP2;1, thereby enhancing the cell's capacity for osmotic water uptake and further contributing to the maintenance of intracellular thermal homeostasis[31,33]. Diacylglycerol kinase 7 (DGK7) responds to heat at the plasma membrane by sensing the accumulation of DAG, lay the foundation for temperature homeostasis in the cytoplasm. Within 10–60 min of heat stress, fatty acid desaturases are strongly upregulated, markedly increasing the proportion of tri-unsaturated fatty acids in both plasma and organelle membranes. This shift increases the membrane fluidity and facilitated the exchange of substances and thermal energy at different temperatures between the inside and outside of the cell, and organelles[47].

Most strikingly, chloroplasts-highly thermosensitive yet essential organelles-maintain remarkably stable temperatures even under drastic environmental fluctuations, typically within 1.5 °C despite 40 °C changes in air temperature. Because chloroplast enzymes are exquisitely temperature-sensitive, this thermal homeostasis is crucial for sustaining physiological activity. Although the precise mechanisms remain unclear, their deep cellular localization buffers incoming heat through the surrounding cytoplasm, while active responses-including rapid Ca^{2+}-mediated solute influx that enhances aquaporin-driven water permeability, preserving chloroplast function within a narrow thermal range.

Under heat stress, plants rapidly activate a negative-feedback thermal regulation loop in which heat perception triggers stomatal opening, aquaporin activation, membrane lipid remodeling, and the induction of heat-shock proteins. These coordinated responses enhance transpiration, increase membrane water permeability and fluidity, collectively leading to leaf cooling and mitigation of heat damage. This feedback mechanism allows plants to rapidly counteract transient high-

temperature stress, stabilizing leaf temperature and protecting temperature-sensitive physiological processes, such as photosynthesis.

In conclusion, our findings provide direct evidence that plants maintain thermal homeostasis through multiscale, hierarchical temperature regulation. This work establishes a conceptual framework linking cellular and subcellular organization to temperature control and has important implications for understanding plant adaptation to climate change, as well as for developing thermally resilient crops. The discovery of active, multi-tiered temperature regulation at subcellular scales reveals an unexpected level of plant homeostatic sophistication and challenges traditional views of plant thermal adaptation.

Methods

Photochemical synthesis of L-AuNP@HTT

Typically, $HAuCl_4$ (10 mM, 1.0 mL) ethanol solution and NaOH ethanol solution (0.2 M, 200 μL) were mixed with HTT solution (20 μM, 4.82 mg in 9.0 mL trichloromethane). After stirring the mixture for 15 min at 25°C, the reaction system was irradiated with an 8-W 390-nm lamp for 60 h. Then, the reaction mixture was converted into cold ethanol quickly and kept in the refrigerator (4°C) until no further pale green precipitate formed. This precipitate was carefully collected by centrifugation at 4000 rpm for 15 min and washed three times with anhydrous ethanol. The final product of L-AuNP@HTT was dried in a vacuum oven for further studies[48].

The synthesis of p-AuNPs via polymer encapsulation of L-AuNP@HTT

One milliliter PMMA-co-MAA copolymer (1:0.016 (methyl methacrylate: methacrylic acid), average Mw ~ 34,000 by GPC, average Mn ~ 15,000 by GPC) solution in tetrahydrofuran (THF, 1.0 mg mL^{-1}) and 1.0 mL L-AuNP@HTT solution in tetrahydrofuran (1.0 mg mL^{-1}) were first mixed and then added slowly into a 20 mL ultrapure water under stirring at 37°C, drop by drop. The mixture was then stirred for about 10 min, yielding a transparent colloidal solution. The tetrahydrofuran was removed by the vacuum rotary evaporation at 45°C, and the precipitate was obtained by centrifugation. The prepared nanoparticles (namely p-AuNPs) could be well dispersed in water[48].

Characterization of p-AuNP@HTT.

The morphology of p-AuNPs was characterized by transmission electron microscopy (TEM, JEM-2100F). Particle diameters were measured for at least 200 individual particles using ImageJ software, and the mean core size and polydispersity index were determined by Gaussian fitting of the size distribution histogram.

Optical properties of p-AuNs (80 μg/mL, 3 mL) were measured in a quartz cuvette at 25°C using an F-4500 spectrophotometer, with ultrapure water as the blank reference. UV–vis absorption spectra were recorded over 200–800 nm at 1 nm resolution. For fluorescence measurements, the emission spectrum was acquired from 430 to 750 nm under 405 nm excitation, and the excitation spectrum was recorded from 300 to 500 nm with a fixed emission wavelength of 529 nm.

Fluorescence lifetime measurements were performed on a DeltaFlex time-correlated single-photon counting spectrometer. Samples (80 μg/mL) were excited at 405 nm at 25.0 ± 0.1°C, and data were collected until the peak channel count reached 10^4. Raw decay data were corrected using Fluoracle software and fitted in Origin 2025 to a three-exponential decay model: $I(t) = B_1\exp(-t/\tau_1) +$

$B_2\exp(-t/\tau_2) + B_3\exp(-t/\tau_3)$, where Bn and τ_n are the amplitude and lifetime of each component, respectively. The intensity-weighted average lifetime was calculated as $\langle\tau\rangle = (\Sigma B_n\tau_n^2)/(\Sigma B_n\tau_n)$. Goodness of fit was assessed by $\chi^2 < 1.2$ and the distribution of weighted residuals.

Temperature-dependent fluorescence was measured using an FLS980 fluorescence spectrometer equipped with a circulating thermostat (accuracy: ± 0.1°C). A linear temperature gradient from 0 to 60°C was applied in 5°C increments; each temperature point was equilibrated for 10 min prior to spectral acquisition. Emission spectra (450–700 nm) were recorded under 405 nm excitation, and the peak fluorescence intensity was plotted as a function of temperature.

Photostability was evaluated using a custom-built time-gated imaging system. p-AuNPs (80 µg/mL, 3 mL) was excited by an OBIS LX 405 nm pulsed laser. Fluorescence intensity was recorded continuously for 1200 s at 1 s intervals using an ICCD camera (PI MAX4) with a delay time of 100 ns and a gate width of 60 ns.

The effect of pH on fluorescence intensity was assessed by adjusting p-AuNPs solutions to pH 5.0 – 10.0[49-51]using phosphate buffers of appropriate pH, with actual pH values confirmed by a calibrated pH meter. Emission peak fluorescence intensities were measured using an F-4500 spectrophotometer (λ_{ex} = 405 nm).

The influence of physiologically relevant ions on probe fluorescence was examined by adding $CaCl_2$, $MgCl_2$, NaCl, or KCl stock solutions to p-AuNPs to achieve a series of ion concentrations spanning the physiological range in plants[16,52-54]. Emission spectra (450–650 nm) were recorded at each concentration using an F-4500 spectrophotometer (λ_{ex} = 405 nm), and peak fluorescence intensities were compared to untreated controls.

The stability of p-AuNPs fluorescence in the presence of hydrogen peroxide was examined over the physiologically relevant concentration range. H_2O_2 stock solution was added to p-AuNPs[55] (80 µg mL^{-1}) to achieve final concentrations of 0-10^{-1} mol L^{-1}. Emission spectra (450–650 nm) were recorded using an F-4500 spectrophotometer (λ_{ex} = 405 nm), and peak fluorescence intensities were compared to the untreated control.

Phytotoxicity of p-AuNPs was evaluated in approximately 4-week-old tobacco plants. Using a 1 mL syringe, 20 µL of p-AuNPs (80 µg mL^{-1}) or 20 µL of ddH_2O (control) was infiltrated into the abaxial surface of separate leaves, and injection sites were marked. Leaf morphology was recorded at 0 h, 1 h, and 7 days post-infiltration to assess any signs of phytotoxicity.

Time-gated imaging system.

A schematic of the installations used for time-gated imaging experiments is shown in fig. 1g. The images were obtained with an objective (20×, L-Plan, NA 0.40, SHPQYQ) passed through an optical long-pass filter (GCC-300114, Daheng Optics), and an intensified CCD detector (ICCD) (PI-MAX4, Princeton Instruments). And a laser of 405 nm (OBIS 405 LX, Coherent) with a repetition rate of 500 k Hz was used as an excitation source. The gating parameters were controlled with a digital delay generator (DG535, Stanford Research Systems) via a GPIB interface. To obtain the best image focus during imaging scanning, auto focusing was carried out by using precision electronically controlled translation table (GCD-202050M, Daheng Optics). Custom LabView software (National Instruments) was developed in-house for complete instrumental control and data collection. A minimal gate of 100 ns was used for most applications.

The scheme of plants temperature detection was shown in figure 1. p-AuNP@HTT were used as nanothermometers for subsequent experiments. Three plants, *N.benthamiana*, and *Arabidopsis*

were utilized in our system. All experiments were performed on the intact leaves of 4-week-old plants, with the plants incubated in the growth chamber. The p-AuNPs aqueous solution were administered into the 3rd or 4th leaf of the plant by pressing a 1-mL needleless syringe onto the abaxial side of the leaves, 20-50 μL (80 μg mL^{-1}) for each leaf. Then, by using the TGI system, the PL signal from these p-AuNPs probes could be acquired. Meanwhile, the autofluorescence from the leaves and the excitation background noise were effectively eliminated. Based on the temperature-dependent intensity of these p-AuNPs, the relative temperature changes in leaf (ΔT_{leaf}) could be detected.

In a typical TGI system, a pulsed light source (OBIS 405 LX, Coherent, with a repetition rate of 500k Hz) was used to excite the target p-AuNPs probe. As shown in fig. S6, while exciting the desired long-lived luminescence signals of p-AuNPs, undesired short-lived luminescence signals of the autofluorescence from the bio-sample matrix are also induced. To remove this interference, the detector was kept off for a period of time (TG delay). Then the detection was turned on after a brief delay once the undesired signals have nearly disappeared. It can be turned off when the desired signals are mostly collected. The process described above is typically repeated multiple times to collect more desired signals from the target probe. This can greatly increase the signal-to-noise ratio (SNR)[56]. In particular, it is important to consider the different photostability of autofluorescence and target fluorescence signals in practical applications. High photostability is desirable for target probes as they are more resistant to photobleaching[57]. The TGI technique, combined with long-lived and temperature-sensitive photoluminescence probes, offers a novel approach to effectively eliminate the interference of background noise from autofluorescence and thus make possible for reliable study of plant thermoregulation.

As shown in fig. S6, when the time delay was set to 0 ns, the autofluorescence of the leaves and the signals of p-AuNPs could not be distinguished. For comparison, when the time delay was set to 100 ns, the autofluorescence could be completely removed, and only the signal of p-AuNPs within the leaves could be accurately obtained. Then, we changed the temperature around the plant and at the same time recorded the fluorescence intensity of the p-AuNPs in the leaves as a function of temperature in real time to resolve the response of the internal temperature of the plant to the air temperature.

Plant materials and growth conditions.

Nicotiana benthamiana was used as the wild type. Surface-sterilized seeds were germinated on half-strength Murashige and Skoog medium. The seeds were kept at 4°C for 2 days and then transferred to a greenhouse under long-day conditions (16 hours light, 8 hours dark, and constant 22°C). Seedlings were transferred to soil 7 days after plating. Plants were grown at 22°C with a 16/8-h light/dark cycle.

Arabidopsis thaliana was grown under conditions as described in *Arabidopsis* ecotype Columbia (Col-0) was used as the wild type. Seeds were surface-sterilized for 12 min in 10% kitchen bleach. After washing five times with sterile water, seeds were plated on 1/2 Murashige and Skoog (MS) medium. The plates were stratified at 4°C for 2 d in the dark and were then transferred to a growth chamber at 22°C with a 16-h light/8-h dark photoperiod (light intensity, 120 μmol photons m^{-2} s^{-1}).

Tomato (*S. lycopersicum* 'Ailsa Craig') seeds were germinated on wet filter paper and transferred to the aperture disc filled with a mixture of peat: vermiculite (2:1, v/v). The seedlings were grown under a 16-h light/8-h dark photoperiod with the temperature of 26°C in phytotron.

All experiments were performed on the intact leaves of 4-week-old plants, with the plants incubated in the growth chamber until the time of data collection. Young leaves (*N.benthamiana*: approximately 2 cm × 3 cm in size; *Arabidopsis*: approximately 1 cm × 2 cm in size; Tomato*:* approximately 1 cm × 1.5 cm in size) were infiltrated using a 1-mL needleless syringe on the abaxial side of the leaves.

Temperature calibration and conversion from p-AuNP fluorescence intensity.

To convert the fluorescence intensity of p-AuNPs to internal leaf temperature, we first established the temperature-dependent fluorescence response of the probes in planta. The relative change in fluorescence intensity (ΔI) of p-AuNPs infiltrated into plants leaves was measured as a function of ambient temperature under controlled conditions. ΔI was calculated as the relative intensity change using the equation:

$$\Delta I \text{ (relative intensity, \%)} = (I - I_0) / I_0 \times 100\% \quad (1)$$

where I is the fluorescence intensity at a given temperature and I_0 is the reference intensity measured at the initial temperature (typically 24°C).

The temperature sensitivity of p-AuNP fluorescence in leaf tissues exhibited a linear relationship over the tested range, described by the calibration equation:

$$y = -1.22\ x + 104.41\ (R^2 = 0.993) \quad (2)$$

where y represents the relative fluorescence intensity (%) and x is the temperature (°C). This linear fit was derived from averaged measurements across multiple independent infiltrations and temperature ramps (see Fig. 1a).

The relative temperature change (ΔT) in the leaf was then calculated from the observed relative change in fluorescence intensity (I, %) using the inverse relationship:

$$\Delta T\ (°C) = \Delta I / 1.22 \quad (3)$$

This sensitivity factor (1.22 % per °C) corresponds to the absolute value of the slope from the calibration equation. All fluorescence intensities were background-corrected using time-gated imaging to eliminate autofluorescence contributions, as described above.

References

1 Zhao, C. *et al.* Temperature increase reduces global yields of major crops in four independent estimates. *Proceedings of the National Academy of Sciences* **114**, 9326-9331, doi:10.1073/pnas.1701762114 (2017).

2 Ding, Y. & Yang, S. Surviving and thriving: How plants perceive and respond to temperature stress. *Developmental Cell* **57**, 947-958, doi:10.1016/j.devcel.2022.03.010 (2022).

3 Andaya, V. C. Mapping of QTLs associated with cold tolerance during the vegetative stage in rice. *Journal of Experimental Botany* **54**, 2579-2585, doi:10.1093/jxb/erg243 (2003).

4 Still, C. J. *et al.* No evidence of canopy-scale leaf thermoregulation to cool leaves below air temperature across a range of forest ecosystems. *Proceedings of the National Academy of Sciences* **119**, e2205682119, doi:10.1073/pnas.2205682119 (2022).

5 Drake, J. E. *et al.* No evidence of homeostatic regulation of leaf temperature in Eucalyptus parramattensis trees: integration of CO2 flux and oxygen isotope methodologies. *New Phytologist* **228**, 1511-1523, doi:10.1111/nph.16733 (2020).

6 Yamasaki, T. *et al.* Temperature Acclimation of Photosynthesis and Related Changes in Photosystem II Electron Transport in Winter Wheat. *Plant Physiology* **128**, 1087-1097, doi:10.1104/pp.010919 (2002).

7 Penfield, S. Temperature perception and signal transduction in plants. *New Phytologist* **179**,

615-628, doi:10.1111/j.1469-8137.2008.02478.x (2008).

8 Argyris, J. *et al.* Quantitative trait loci associated with seed and seedling traits in Lactuca. *Theoretical and Applied Genetics* **111**, 1365-1376, doi:10.1007/s00122-005-0066-4 (2005).

9 Mahan, J. R. & Upchurch, D. R. Maintenance of constant leaf temperature by plants—I. Hypothesis-limited homeothermy. *Environmental and Experimental Botany* **28**, 351-357, doi:10.1016/0098-8472(88)90059-7 (1988).

10 Claudel, C., Loiseau, O., Silvestro, D., Lev-Yadun, S. & Antonelli, A. Patterns and drivers of heat production in the plant genus Amorphophallus. *The Plant Journal* **115**, 874-894, doi:10.1111/tpj.16343 (2023).

11 Michaletz, S. T. *et al.* Plant Thermoregulation: Energetics, Trait–Environment Interactions, and Carbon Economics. *Trends in Ecology & Evolution* **30**, 714-724, doi:10.1016/j.tree.2015.09.006 (2015).

12 Savvides, A., van Ieperen, W. I. M., Dieleman, J. A. & Marcelis, L. F. M. Meristem temperature substantially deviates from air temperature even in moderate environments: is the magnitude of this deviation species-specific? *Plant, Cell & Environment* **36**, 1950-1960, doi:10.1111/pce.12101 (2013).

13 Michaletz, S. T. *et al.* The energetic and carbon economic origins of leaf thermoregulation. *Nature Plants* **2**, doi:10.1038/nplants.2016.129 (2016).

14 Yang, F. *et al.* Measurement of local temperature increments induced by cultured HepG2 cells with micro-thermocouples in a thermally stabilized system. *Scientific Reports* **7**, doi:10.1038/s41598-017-01891-1 (2017).

15 Costa JM, Grant OM, Chaves MM. Thermography to explore plant-environment interactions. J Exp Bot. **64**, 3937-49. doi:10.1093/jxb/ert029 (2013).

16 Zhou, J., del Rosal, B., Jaque, D., Uchiyama, S. & Jin, D. Advances and challenges for fluorescence nanothermometry. *Nature Methods* **17**, 967-980, doi:10.1038/s41592-020-0957-y (2020).

17 Zhou, J., Del Rosal, B., Jaque, D., Uchiyama, S. & Jin, D. Advances and challenges for fluorescence nanothermometry. *Nat Methods* **17**, 967-980, doi:10.1038/s41592-020-0957-y (2020).

18 Okabe, K. *et al.* Intracellular temperature mapping with a fluorescent polymeric thermometer and fluorescence lifetime imaging microscopy. *Nat Commun* **3**, 705, doi:10.1038/ncomms1714 (2012).

19 Meyer, R. A. Light scattering from biological cells: dependence of backscatter radiation on membrane thickness and refractive index. *Applied optics* **18**, 585-588 (1979).

20 Dey, P. M. & Harborne, J. B. *Plant biochemistry*. (Elsevier, 1997).

21 Knight, M. R., Campbell, A. K., Smith, S. M. & Trewavas, A. J. Transgenic plant aequorin reports the effects of touch and cold-shock and elicitors on cytoplasmic calcium. *Nature* **352**, 524-526 (1991).

22 Xue, Y. *et al.* Aggregation-induced emission: the origin of lignin fluorescence. *Polymer Chemistry* **7**, 3502-3508 (2016).

23 Blonder, B. & Michaletz, S. T. A model for leaf temperature decoupling from air temperature. *Agricultural and Forest Meteorology* **262**, 354-360, doi:10.1016/j.agrformet.2018.07.012 (2018).

24 Michaletz, S. T. *et al.* The energetic and carbon economic origins of leaf thermoregulation. *Nat Plants* **2**, 16129, doi:10.1038/nplants.2016.129 (2016).

25 Dong, N., Prentice, I. C., Harrison, S. P., Song, Q. H. & Zhang, Y. P. Biophysical homoeostasis of leaf temperature: A neglected process for vegetation and land-surface modelling. *Global Ecology and Biogeography* **26**, 998-1007, doi:10.1111/geb.12614

(2017).

26 Drake JE, Harwood R, Vårhammar A, Barbour MM, Reich PB et al. No evidence of homeostatic regulation of leaf temperature in Eucalyptus parramattensis trees: integration of CO2 flux and oxygen isotope methodologies. *New Phytol* **228**,1511-1523. doi: 10.1111/nph.16733(2020).

27 Hayes, S., Schachtschabel, J., Mishkind, M., Munnik, T. & Arisz, S. A. Hot topic: Thermosensing in plants. *Plant Cell Environ* **44**, 2018-2033, doi:10.1111/pce.13979 (2021).

28 Kan, Y., Mu, X. R., Gao, J., Lin, H. X. & Lin, Y. The molecular basis of heat stress responses in plants. *Mol Plant* **16**, 1612-1634, doi:10.1016/j.molp.2023.09.013 (2023).

29 Li, D., Zhu, Z. & Sun, D. W. Visualization and quantification of content and hydrogen bonding state of water in apple and potato cells by confocal Raman microscopy: A comparison study. *Food Chem* **385**, 132679, doi:10.1016/j.foodchem.2022.132679 (2022).

30 Giuliani, N. *et al.* Impact of soil water availability on apple tree physiology during heatwaves and on post-stress recovery. *Environmental and Experimental Botany* **235**, doi:10.1016/j.envexpbot.2025.106161 (2025).

31 Yaaran, A. & Moshelion, M. Role of Aquaporins in a Composite Model of Water Transport in the Leaf. *Int J Mol Sci* **17**, doi:10.3390/ijms17071045 (2016).

32 Mills, C., Bartlett, M. K. & Buckley, T. N. The Stomatal Response to Temperature Is Enhanced by High Evaporative Demand, Consistent With a Partially Hydraulic Mechanism. *Plant Cell Environ* **49**, 1958-1968, doi:10.1111/pce.70347 (2026).

33 Grondin, A. *et al.* Aquaporins Contribute to ABA-Triggered Stomatal Closure through OST1-Mediated Phosphorylation. *Plant Cell* **27**, 1945-1954, doi:10.1105/tpc.15.00421 (2015).

34 Legris, M. *et al.* Phytochrome B integrates light and temperature signals in *Arabidopsis*. *Science* **354**, 897-900, doi:10.1126/science.aaf5656 (2016).

35 Bohn, L. *et al.* The temperature sensor TWA1 is required for thermotolerance in Arabidopsis. *Nature* **629**, 1126-1132, doi:10.1038/s41586-024-07424-x (2024).

36 Li, J. & Song, Y. Plant thermosensors. *Plant Sci* **342**, 112025, doi:10.1016/j.plantsci.2024.112025 (2024).

37 Kool, D. *et al.* A review of approaches for evapotranspiration partitioning. *Agricultural and Forest Meteorology* **184**, 56-70, doi:10.1016/j.agrformet.2013.09.003 (2014).

38 Xiang, K., Li, Y., Horton, R. & Feng, H. Similarity and difference of potential evapotranspiration and reference crop evapotranspiration – a review. *Agricultural Water Management* **232**, doi:10.1016/j.agwat.2020.106043 (2020).

39 Devireddy, A. R., Tschaplinski, T. J., Tuskan, G. A., Muchero, W. & Chen, J. G. Role of Reactive Oxygen Species and Hormones in Plant Responses to Temperature Changes. *Int J Mol Sci* **22**, doi:10.3390/ijms22168843 (2021).

40 Garen, J. C. & Michaletz, S. T. Temperature governs the relative contributions of cuticle and stomata to leaf minimum conductance. *New Phytol* **245**, 1911-1923, doi:10.1111/nph.20346 (2025).

41 Chua, L. C. & Lau, O. S. Stomatal development in the changing climate. *Development* **151**, doi:10.1242/dev.202681 (2024).

42 Zhang, Y. *et al.* Arabidopsis HSFA1b functions as a heat sensor inhibiting OST1-mediated stomatal closure through its adenylate-cyclase activity. *Molecular Plant* **18**, 1549-1566, doi:10.1016/j.molp.2025.07.018 (2025).

43 Kollist, H., Nuhkat, M. & Roelfsema, M. R. Closing gaps: linking elements that control stomatal movement. *New Phytol* **203**, 44-62, doi:10.1111/nph.12832 (2014).

44 Pankasem, N., Hsu, P. K., Lopez, B. N. K., Franks, P. J. & Schroeder, J. I. Warming triggers

stomatal opening by enhancement of photosynthesis and ensuing guard cell CO_2 sensing, whereas higher temperatures induce a photosynthesis-uncoupled response. *New Phytol* **244**, 1847-1863, doi:10.1111/nph.20121 (2024).

45 Lenzoni, G. & Knight, M. R. Increases in Absolute Temperature Stimulate Free Calcium Concentration Elevations in the Chloroplast. *Plant Cell Physiol* **60**, 538-548, doi:10.1093/pcp/pcy227 (2019).

46 Alhaithloul, H. A., Soliman, M. H., Ameta, K. L., El-Esawi, M. A. & Elkelish, A. Changes in Ecophysiology, Osmolytes, and Secondary Metabolites of the Medicinal Plants of Mentha piperita and Catharanthus roseus Subjected to Drought and Heat Stress. *Biomolecules* **10**, doi:10.3390/biom10010043 (2019).

47 Kan, Y. *et al.* A stepwise decoding mechanism for heat sensing in plants connects lipid remodeling to a nuclear signaling cascade. *Cell* **188**, 7378-7396 e7323, doi:10.1016/j.cell.2025.11.003 (2025).

48 Yang, L. *et al.* Highly luminescent gold nanoparticles prepared via a facile photochemical method for bioimaging applications. *Advanced Composites and Hybrid Materials* **7**, doi:10.1007/s42114-024-00964-w (2024).

49 Martiniere, A. *et al.* Uncovering pH at both sides of the root plasma membrane interface using noninvasive imaging. *Proc Natl Acad Sci U S A* **115**, 6488-6493, doi:10.1073/pnas.1721769115 (2018).

50 Barbez, E., Dünser, K., Gaidora, A., Lendl, T. & Busch, W. Auxin steers root cell expansion via apoplastic pH regulation in Arabidopsis thaliana. *Proceedings of the National Academy of Sciences* **114**, doi:10.1073/pnas.1613499114 (2017).

51 Zondervan, R., Kulzer, F., van der Meer, H., Disselhorst, J. A. & Orrit, M. Laser-driven microsecond temperature cycles analyzed by fluorescence polarization microscopy. *Biophys J* **90**, 2958-2969, doi:10.1529/biophysj.105.075168 (2006).

52 Stael, S. *et al.* Plant organellar calcium signalling: an emerging field. *J Exp Bot* **63**, 1525-1542, doi:10.1093/jxb/err394 (2012).

53 Lenzoni, G. & Knight, M. R. Increases in Absolute Temperature Stimulate Free Calcium Concentration Elevations in the Chloroplast. *Plant and Cell Physiology* **60**, 538-548, doi:10.1093/pcp/pcy227 (2018).

54 Tan, M. *et al.* Accurate In Vivo Nanothermometry through NIR-II Lanthanide Luminescence Lifetime. *Small (Weinheim an der Bergstrasse, Germany)* **16**, e2004118, doi:10.1002/smll.202004118 (2020).

55 Suzuki, N. & Katano, K. Coordination Between ROS Regulatory Systems and Other Pathways Under Heat Stress and Pathogen Attack. *Front Plant Sci* **9**, 490, doi:10.3389/fpls.2018.00490 (2018).

56 Yang, W. & Chen, S.-L. Time-gated fluorescence imaging: Advances in technology and biological applications. *Journal of Innovative Optical Health Sciences* **13**, doi:10.1142/s1793545820300062 (2020).

57 Yang, W. & Chen, S.-L. Time-gated fluorescence imaging: Advances in technology and biological applications. *Journal of Innovative Optical Health Sciences* **13**, 2030006 (2020).

Notes

Acknowledgments:

We would like to express our gratitude to Prof. Xiaofeng Cao, Prof. Yongbiao Xue and Prof. Wenxiang Meng (Institute of Genetics and Developmental Biology, CAS) for their invaluable suggestions; Prof. Weicai Yang (Institute of Genetics and Developmental Biology, CAS) for

providing the *Arabidopsis thaliana* (Col-0) seeds used in this study; Prof. Zhixi Tian (Institute of Genetics and Developmental Biology, CAS) for providing the *Nicotiana benthamiana* seeds used in this study; Chuanyou Li (Shandong agricultural university, SDAU) for providing the *Tomato* ('Ailsa Craig') seeds used in this study; Prof. Guodong Wang (Institute of Genetics and Developmental Biology Shandong agricultural university, CAS) for his assistance in utilizing the plant growth facility.

Funding:

This work was supported by the National Natural Science Foundation of China (Grant Numbers: 2024YFA1209900, 82050006 and 62175257) and the Strategic Priority Research Program of CAS (Grant No. XDA24020202-1)

Author contributions:

XC, CL, DYZ, YXW and YQJ carried out the experiments, RCH, FHY and XC designed and synthesized thermal sensors, LH, YQQ, CL and XYW built the setup, CL, XC and YQJ performed the modelling and simulation, XC, CL, RCH and YQJ wrote the MS, and all the authors attended the data analysis and paper revision. This work was initialed by RCH, LH, YW and YQJ, and supervised by YQJ.

Competing interests:

Authors declare that they have no competing interests.

Data and materials availability:

All data are available in the main text or the supplementary materials.

Supplementary Materials

Supplementary Text

Figs. S1 to S12

Supplementary Files

This is a list of supplementary files associated with this preprint. Click to download.

- SupplementaryInformation.pdf